An implicit finite-element model for 3D non-hydrostatic mesoscale ocean flows

M.A. Maidana[1], J. Blasco[2], M. Espino[1]

[1] *Laboratorio de Ingeniería Marítima, Univ. Politècnica de Catalunya*
Campus Nord, Edfici D1,
c/Gran Capità s/n, 08034 Barcelona (Spain)

[2] *Dept. de Matemàtica Aplicada I, Univ. Politècnica de Catalunya*
Campus Sud, Edfici H,
Avgda. Diagonal 647, 08028 Barcelona (Spain)

SUMMARY

We present in this paper a pressure stabilized, finite element method for the numerical approximation of three-dimensional, non-hydrostatic mesoscale ocean flows. The model considered here incorporates surface wind stress, bottom friction and Coriolis acceleration, and it is applicable to irregular bottom topographies. An implicit unconditionally stable scheme is employed for the time advancement and an anisotropic stabilization technique is used for the spatial finite element discretization. The numerical results obtained on test cases demonstrate the robustness and accuracy of the method proposed here. mycopyright

KEY WORDS: Ocean Modelling Navier-Stokes equations Non-hydrostatic flows Finite elements

1 INTRODUCTION

Improvements in computations have made numerical codes more and more useful in Oceanographic Engineering and the idea of using unstructured grids for modelling mesoscale ocean dynamics sounds very attractive given the high complexity of the ocean geometry. Fine topographic features like narrow straits, steep continental slopes, islands, etc... are of crucial importance and may control the circulation on mesoscale spatial scales, while they can hardly be resolved with an affordable homogeneous spatial resolution. The finite element method (FEM) offers a traceable tool to tackle this problem (see, e.g., [14]).

Attractiveness of the FEM for modelling ocean dynamics was demonstrated more at the dawn of the age of ocean circulation modelling by Fix ([18]). Such nice properties of the FEM as conservation of energy, which is common to all variational methods of solving differential equations, natural treatment of boundary conditions and flexibility of triangulation were complemented with availability of supercomputers. Having these in mind, Le Provost ([25]) suggested this approach as an interesting alternative to the finite difference method commonly used in ocean modelling.

Several simplified FEM numerical models have been derived from the hydrostatic Navier-Stokes equations to study specific flow in a determinate scale. Thus, for example,

the two-dimensional vertically averaged shallow water equations are commonly used to study the circulation in well-mixed shallow estuaries, coastal seas and lakes (see, e.g., [15], [16], [17], [26], [28], [29], [33]). Other frequently used hydrostatic models employ the so called primitive equations of the ocean (see, e.g., [9], [14], [23]). However, the hydrostatic approximation is not always valid in flows over rapidly varying slopes, such as littoral areas (see [7]).

On the other hand, some non-hydrostatic numerical ocean models have also been developed recently (see, e.g., [7], [24], [27], [30], [31], [32] and the references therein). All of these models, however, use the finite difference method for the spatial approximation, with a careful choice of the position of the velocity and pressure degrees of freedom on different cell locations.

High resolution of ocean flows can certainly be obtained by solving numerically the three-dimensional non-hydrostatic incompressible Navier-Stokes equations. This flow problem, however, presents several numerical difficulties, the main one being associated to possible pressure instabilities originated from the treatment of the incompressibility condition. Moreover, if the finite element method is employed in a z-coordinate formulation, the difference between the horizontal and the vertical scales in coastal seas may result in highly anisotropic meshes, with elements having large aspect ratios.

We present in this paper a three-dimensional non-hydrostatic pressure-stabilized finite element ocean model, which incorporates a fully implicit time stepping scheme. An anisotropic pressure stabilization technique is employed in our model. A diagnostic formulation, in which the density is assumed to be known, is considered at the present stage of development.

The outline of the paper is as follows: Section 2 introduces the hydrodynamical problem to approximate and some notation. In Section 3, the stabilized numerical method used is described, first accounting for the time discretization procedure and then introducing the finite element spatial approximation. Numerical results are presented in Section 4, whereas in Section 5 conclusions are drawn.

2 HYDRODYNAMICAL MODEL

We consider the turbulent flow of a three-dimensional, incompressible fluid in a domain $\Omega \subset \mathbb{R}^3$, expressed in a rotating Cartesian coordinate system and under the acceleration due to gravity. Assuming the Boussinesq approximation, the fluid density is considered constant except in the gravity acceleration term of the equations of motion, thus accounting for buoyancy effects. After averaging the Navier-Stokes equations over turbulent time-scales, the momentum and continuity equations reflecting the physical principles of conservation of momentum and mass become:

$$\frac{\partial u}{\partial t} + u\frac{\partial u}{\partial x} + v\frac{\partial u}{\partial y} + w\frac{\partial u}{\partial z} - fv + \frac{\partial p}{\partial x} - \frac{\partial}{\partial x}(\nu_H\frac{\partial u}{\partial x}) - \frac{\partial}{\partial y}(\nu_H\frac{\partial u}{\partial y}) - \frac{\partial}{\partial z}(\nu_V\frac{\partial u}{\partial z}) = 0 \quad \text{in } \Omega\times(0,T) \tag{1}$$

$$\frac{\partial v}{\partial t} + u\frac{\partial v}{\partial x} + v\frac{\partial v}{\partial y} + w\frac{\partial v}{\partial z} + fu + \frac{\partial p}{\partial y} - \frac{\partial}{\partial x}(\nu_H\frac{\partial v}{\partial x}) - \frac{\partial}{\partial y}(\nu_H\frac{\partial v}{\partial y}) - \frac{\partial}{\partial z}(\nu_V\frac{\partial v}{\partial z}) = 0 \quad \text{in } \Omega\times(0,T) \tag{2}$$

$$\frac{\partial w}{\partial t} + u\frac{\partial w}{\partial x} + v\frac{\partial w}{\partial y} + w\frac{\partial w}{\partial z} + \frac{\partial p}{\partial z} - \frac{\partial}{\partial x}(\nu_H\frac{\partial w}{\partial x}) - \frac{\partial}{\partial y}(\nu_H\frac{\partial w}{\partial y}) - \frac{\partial}{\partial z}(\nu_V\frac{\partial w}{\partial z}) = -\frac{\rho}{\rho_0}g \quad \text{in } \Omega\times(0,T) \tag{3}$$

$$\frac{\partial u}{\partial x} + \frac{\partial v}{\partial y} + \frac{\partial w}{\partial z} = 0 \quad \text{in } \Omega\times(0,T) \tag{4}$$

Here, $u(x,y,z,t)$, $v(x,y,z,t)$ and $w(x,y,z,t)$ are the fluid velocity components in the horizontal $x-$ and $y-$ and vertical $z-$directions, respectively; t is the time, T being a given final time; $p(x,y,z,t)$ is the fluid kinematic pressure, that is, the pressure divided by the reference density ρ_0; $f = 2\omega\sin(\phi)$ is the Coriolis parameter, ω being the Earth's angular velocity and ϕ the latitude of the region of interest; g is the gravitational acceleration; ν_H and ν_V are the horizontal and vertical turbulent eddy viscosities, respectively, which are obtained from an appropriate turbulence closure model (a given constant value is assumed here); finally, $\rho(x,y,z,t)$ is the fluid density. A diagnostic model is considered at the present stage of development of the model, in which ρ is a prescribed positive function of the spatial coordinates.

It should be noted that the model just described is non-hydrostatic, in the sense that the pressure is not assumed to vary linearly with depth, as opposed to extensively used hydrostatic models such as shallow water or primitive equation models. The hydrostatic approximation is not always valid in flows over rapidly varying slopes, such as those of coastal areas.

The equation system (1)-(2)-(3)-(4)- can also be written in vector form as follows:

$$\frac{\partial \mathbf{u}}{\partial t} + (\mathbf{u}\cdot\nabla)\mathbf{u} + f\,\mathbf{k}\times\mathbf{u} + \nabla p - \frac{\partial}{\partial x}(\nu_H\frac{\partial \mathbf{u}}{\partial x}) - \frac{\partial}{\partial y}(\nu_H\frac{\partial \mathbf{u}}{\partial y}) - \frac{\partial}{\partial z}(\nu_V\frac{\partial \mathbf{u}}{\partial z}) = -\frac{\rho}{\rho_0}\mathbf{g} \quad \text{in } \Omega\times(0,T) \tag{5}$$

$$\nabla\cdot\mathbf{u} = 0 \quad \text{in } \Omega\times(0,T) \tag{6}$$

where $\mathbf{u} = (u,v,w)$ is the three-dimensional velocity vector, $\nabla = (\frac{\partial}{\partial x}, \frac{\partial}{\partial y}, \frac{\partial}{\partial z})$, $\mathbf{k} = (0,0,1)$ and $\mathbf{g} = (0,0,g)$. The domain Ω is defined by:

$$\Omega = \{(x,y,z)\in\mathbb{R}^3 \,/\, (x,y)\in S,\ -\mathcal{H}(x,y) < z < 0\}$$

where $S \subset \mathbb{R}^2$ is an open, bounded and polygonal domain (the fluid surface) and $\mathcal{H}\colon \bar{S}\to\mathbb{R}$ is a non-negative, smooth function representing the bottom topography. The

boundary of Ω can be decomposed as $\partial\Omega = \Gamma_s \cup \Gamma_b \cup \Gamma_l$, where:

$$\begin{aligned}
\Gamma_s &= S \times 0 && \text{(surface)}\\
\Gamma_b &= \{(x,y,z) \in \mathbb{R}^3 \,/\, (x,y) \in S,\, -\mathcal{H}(x,y) = z\} && \text{(bottom)}\\
\Gamma_l &= \{(x,y,z) \in \mathbb{R}^3 \,/\, (x,y) \in \partial S,\, -\mathcal{H}(x,y) \le z \le 0\} && \text{(lateral boundary)}
\end{aligned}$$

Moreover, Γ_l is also partitioned into an inflow and an outflow boundary:

$$\Gamma_l \;=\; \Gamma_{\text{in}} \cup \Gamma_{\text{out}}$$

Boundary conditions have to supplied to (5)-(6) in order to have a well-posed problem. At the bottom of the domain, no mass flux is imposed together with a linear bottom friction formulation:

$$w \;+\; u\frac{\partial \mathcal{H}}{\partial x} \;+\; v\frac{\partial \mathcal{H}}{\partial y} \;= 0 \qquad \text{on } \Gamma_b \tag{7}$$

$$\nu_H \frac{\partial \mathcal{H}}{\partial x}\left(\frac{\partial u}{\partial x}, \frac{\partial v}{\partial x}\right) + \nu_H \frac{\partial \mathcal{H}}{\partial y}\left(\frac{\partial u}{\partial y}, \frac{\partial v}{\partial y}\right) + \nu_V\left(\frac{\partial u}{\partial z}, \frac{\partial v}{\partial z}\right) = (\tau_b^x, \tau_b^y) := C_b(u,v) \quad \text{on } \Gamma_b \tag{8}$$

where C_b is the linear bottom friction coefficient.

At the fluid surface, a rigid-lid approximation is assumed and prescribed tangent wind stress is imposed:

$$w \;=\; 0 \qquad \text{on } \Gamma_s \tag{9}$$

$$\nu_V\left(\frac{\partial u}{\partial z}, \frac{\partial v}{\partial z}\right) \;=\; (\tau_s^x, \tau_s^y) \;:=\; \frac{\rho_a}{\rho_0} C_s (U_{10}^2 + V_{10}^2)^{1/2} (U_{10}, V_{10}) \quad \text{on } \Gamma_s \tag{10}$$

where ρ_a is the air's density, C_s the surface wind stress coefficient and (U_{10}, V_{10}) is the horizontal wind velocity vector at a reference height of 10m above the surface at the point $(x, y, 0)$.

A prescribed value of the velocity is imposed at the inflow boundary, whereas a no stress condition is considered at the outflow:

$$\mathbf{u} = \mathbf{u}_I \text{ on } \Gamma_{\text{in}} \tag{11}$$

$$\nu_H\, n_x\, \frac{\partial \mathbf{u}}{\partial x} \;+\; \nu_H\, n_y\, \frac{\partial \mathbf{u}}{\partial y} \;+\; \nu_V\, n_z\, \frac{\partial \mathbf{u}}{\partial z} = \mathbf{0} \quad \text{on } \Gamma_{\text{out}} \tag{12}$$

where $\mathbf{u}_I$ is a given inflow velocity and $\mathbf{n} = (n_x, n_y, n_z)$ is the unit outward normal vector to Γ_{out}.

An initial condition should also be specified for the velocity field:

$$\mathbf{u}(x,y,z,0) \;=\; \mathbf{u}^0(x,y,z), \quad \forall (x,y,z) \in \Omega$$

where $\mathbf{u}^0$ is a given three-dimensional, divergence-free initial velocity.

In order to obtain the weak form of (5), the test function $\tilde{\mathbf{u}} = (\tilde{u}, \tilde{v}, \tilde{w})$ is assumed to vanish on Γ_{in} and be such that $\tilde{w} = 0$ on $\Gamma_s \cup \Gamma_b$. Multiplying (5) by $\tilde{\mathbf{u}}$, integrating on Ω and making use of Green's formula and the boundary conditions (8), (10) and (12) yields:

$$\begin{aligned}
\int_\Omega \frac{\partial \mathbf{u}}{\partial t}\, \tilde{\mathbf{u}}\, d\Omega \;&+\; \int_\Omega (\mathbf{u}\cdot\nabla)\mathbf{u}\, \tilde{\mathbf{u}}\, d\Omega \;+\; \int_\Omega f(\mathbf{k}\times\mathbf{u})\tilde{\mathbf{u}}\, d\Omega \;+\; \int_\Omega \nabla p\, \tilde{\mathbf{u}}\, d\Omega\\
&+\; \int_\Omega \Big(\nu_H \frac{\partial \mathbf{u}}{\partial x}\frac{\partial \tilde{\mathbf{u}}}{\partial x} + \nu_H \frac{\partial \mathbf{u}}{\partial y}\frac{\partial \tilde{\mathbf{u}}}{\partial y} + \nu_V \frac{\partial \mathbf{u}}{\partial z}\frac{\partial \tilde{\mathbf{u}}}{\partial z}\Big)\, d\Omega\\
&=\; -\int_\Omega \frac{\rho}{\rho_0}\, \mathbf{g}\, \tilde{\mathbf{u}}\, d\Omega \;+\; \int_{\Gamma_s} (\tau_s^x \tilde{u} + \tau_s^y \tilde{v})\, d\Gamma \;+\; \int_{\Gamma_b} (\tau_b^x \tilde{u} + \tau_b^y \tilde{v})\, d\Gamma
\end{aligned}$$

where (τ_b^x, τ_b^y) are given by (8) and (τ_s^x, τ_s^y) by (10).

The continuity equation (6) is also enforced weakly. In this case, a scalar test function q is considered, so that multiplying (6) by q and integrating on Ω leads to:

$$\int_\Omega (\nabla \cdot \mathbf{u})\, \tilde{q}\, d\Omega \;=\; 0$$

3 NUMERICAL APPROXIMATION

We describe in this Section the numerical scheme that we employ for the approximation of the hydrodynamical problem (5)-(6). We first introduce the time advancement algorithm in a semidiscrete (continuous space) context and then we consider a spatial discretization based on the finite element method.

3.1 Time stepping

It is common practice in non-hydrostatic ocean models to use a fractional-step method as time integration scheme (see, e.g., [7], [24], [27]). In this kind of methods, each time step is decomposed into a number of substeps, generally two (see, for instance, [3], [21], [22]). This way, the hydrostatic flow is split from a non-hydrostatic pressure correction, the computation of which being usually related to the projection of an intermediate, non-divergence-free velocity field onto the space of solenoidal vector fields. However, a splitting error is thus introduced. As an alternative and simpler approach, we employ an implicit backward Euler monolithic method for the time integration of (5)-(6), in which the velocity and the pressure are computed simultaneously. In this scheme, which is unconditionally stable and first order accurate in the time step size, all the terms are treated implicitly but for the convective (nonlinear) term, which is linearized using the value of the velocity at the previous time step as convective velocity. Thus, given a time step size $\Delta t > 0$, and assuming a known approximation $\mathbf{u}^n$ of the velocity at time $t_n = n\,\Delta t$, a new velocity $\mathbf{u}^{n+1}$ and pressure p^{n+1} at t_{n+1} are obtained from:

$$\frac{1}{\Delta t}(\mathbf{u}^{n+1} - \mathbf{u}^n) \;+\; (\mathbf{u}^n \cdot \nabla)\mathbf{u}^{n+1} \;+\; f\,\mathbf{k} \times \mathbf{u}^{n+1} + \;\nabla p^{n+1}$$

$$-\frac{\partial}{\partial x}(\nu_H \frac{\partial \mathbf{u}^{n+1}}{\partial x}) \;-\; \frac{\partial}{\partial y}(\nu_H \frac{\partial \mathbf{u}^{n+1}}{\partial y}) - \frac{\partial}{\partial z}(\nu_V \frac{\partial \mathbf{u}^{n+1}}{\partial z}) = -\frac{\rho}{\rho_0}\mathbf{g} \text{ in } \Omega \qquad (13)$$

$$\nabla \cdot \mathbf{u}^{n+1} \;=\; 0 \qquad \text{in } \Omega \qquad (14)$$

The weak form of the semidiscrete problem (13)-(14) consists in finding $\mathbf{u}^{n+1} = (u^{n+1}, v^{n+1}, w^{n+1})$ (satisfying the boundary conditions (7), (9) and (11)) and p^{n+1} such that, for all test functions $\tilde{\mathbf{u}} = (\tilde{u}, \tilde{v}, \tilde{w})$ and q:

$$\int_\Omega \frac{1}{\Delta t}(\mathbf{u}^{n+1} - \mathbf{u}^n)\, \tilde{\mathbf{u}}\, d\Omega \;+\; \int_\Omega (\mathbf{u}^n \cdot \nabla)\mathbf{u}^{n+1}\, \tilde{\mathbf{u}}\, d\Omega \;+\; \int_\Omega f(\mathbf{k} \times \mathbf{u}^{n+1})\tilde{\mathbf{u}}\, d\Omega$$

$$+ \;\int_\Omega \nabla p^{n+1}\, \tilde{\mathbf{u}}\, d\Omega \;+\; \int_\Omega \Big(\nu_H \frac{\partial \mathbf{u}^{n+1}}{\partial x}\frac{\partial \tilde{\mathbf{u}}}{\partial x} + \nu_H \frac{\partial \mathbf{u}^{n+1}}{\partial y}\frac{\partial \tilde{\mathbf{u}}}{\partial y} + \nu_V \frac{\partial \mathbf{u}^{n+1}}{\partial z}\frac{\partial \tilde{\mathbf{u}}}{\partial z}\Big)\, d\Omega$$

$$= \;-\int_\Omega \frac{\rho}{\rho_0}\,\mathbf{g}\,\tilde{\mathbf{u}}\, d\Omega \;+\; \int_{\Gamma_s} (\tau_s^x \tilde{u} + \tau_s^y \tilde{v})\, d\Gamma \;+\; \int_{\Gamma_b} (\tau_b^x(u^{n+1})\tilde{u} + \tau_b^y(v^{n+1})\tilde{v})\, d\Gamma$$

$$\int_\Omega (\nabla \cdot \mathbf{u}^{n+1})\, q\, d\Omega \;=\; 0$$

3.2 Finite element spatial approximation

3.2.1 Finite element approximation

The semidiscrete problem (13)-(14) is further discretized in space by the finite element method. Let Ω_h be a partition of Ω, of size $h > 0$, into tetrahedral or hexahedral elements. We assume that all elements $K \in \Omega_h$ are the image of a reference element $\hat{K}$ by a polynomial mapping F_K which is affine for tetrahedra and trilinear for hexahedra. The unknowns of the problem are approximated by finite element functions, which are continuous across interelement boundaries and polynomial within each element when expressed in reference variables. We will focus our attention on the case of equal interpolation for the velocity and the pressure, in which both variables are approximated on the same mesh by polynomials of the same degree.

The standard Galerkin approximation to (13)-(14) consists in finding finite element functions $\mathbf{u}_h^{n+1} = (u_h^{n+1}, v_h^{n+1}, w_h^{n+1})$ (satisfying (7), (9) and (11)) and p_h^{n+1} such that, for all discrete test functions $\tilde{\mathbf{u}}_h = (\tilde{u}_h, \tilde{v}_h, \tilde{w}_h)$ and q_h:

$$
\begin{aligned}
\int_\Omega \frac{1}{\Delta t}(\mathbf{u}_h^{n+1} - \mathbf{u}_h^n)\,\tilde{\mathbf{u}}_h\,d\Omega \;&+\; \int_\Omega (\mathbf{u}_h^n \cdot \nabla)\mathbf{u}_h^{n+1}\,\tilde{\mathbf{u}}_h\,d\Omega \\
+\int_\Omega f(\mathbf{k}\times\mathbf{u}_h^{n+1})\tilde{\mathbf{u}}_h\,d\Omega \;&+\; \int_\Omega \nabla p_h^{n+1}\,\tilde{\mathbf{u}}_h\,d\Omega \\
+\int_\Omega (\nu_H \frac{\partial \mathbf{u}_h^{n+1}}{\partial x}\frac{\partial \tilde{\mathbf{u}}_h}{\partial x} \;&+\; \nu_H \frac{\partial \mathbf{u}_h^{n+1}}{\partial y}\frac{\partial \tilde{\mathbf{u}}_h}{\partial y} + \nu_V \frac{\partial \mathbf{u}_h^{n+1}}{\partial z}\frac{\partial \tilde{\mathbf{u}}_h}{\partial z})d\Omega \\
&= -\int_\Omega \frac{\rho}{\rho_0}\,\mathbf{g}\,\tilde{\mathbf{u}}_h\,d\Omega \;+\; \int_{\Gamma_s} (\tau_s^x \tilde{u}_h + \tau_s^y \tilde{v}_h)\,d\Gamma \\
&+ \int_{\Gamma_b} (\tau_b^x(u_h^{n+1})\tilde{u}_h + \tau_b^y(v_h^{n+1})\tilde{v}_h)\,d\Gamma \qquad (15)
\end{aligned}
$$

$$
\int_\Omega (\nabla \cdot \mathbf{u}_h^{n+1})\,\tilde{q}_h\,d\Omega = 0 \qquad (16)
$$

3.2.2 Stabilization

The numerical method given by (15)-(16) may suffer from different sources of instability. The main ones are the following:

• The convective-diffusive character of the equations may lead to the well-known oscillations that appear in advection-diffusion problems (see [6]), specially in convection dominated flows with large values of the Reynolds number Re= $\dfrac{L\,V}{\nu}$ (L is a characteristic lenght of the flow and V a characteristic velocity). Several techniques have been designed to overcome these oscillations; however, the flows of interest in oceanography generally develop at ranges of turbulent eddy viscosities for which stabilization of convection is unnecessary.

• The presence of the Coriolis term arising from a rotating coordinate system may also introduce instabilities for large values of the Ekman number Ek= $\dfrac{\nu}{\omega L^2}$. Techniques have also been studied to avoid these instabilities (see [13]), but once again, at the scales of motion which we consider stabilization of rotation is also unnecessary.

• Finally, the incompressibility constrain (16) on the velocity field poses a severe problem on the treatment of the pressure. It is well known that in standard approximations of incompressible flow problems, the approximating spaces for the velocity and the pressure have to satisfy a compatibility condition, known as LBB or inf-sup condition, in order to yield a stable and convergent method (see [5]). It has to be said that equal order interpolations do not satisfy this compatibility condition. Several combinations of finite element spaces for the velocity and the pressure have been developed which do satisfy it, but stabilized formulations ([1], [4], [8], [19], [20]) which do not require a compatibility condition have proven to be more efficient than stable mixed pairs. In this alternative approach, some terms are added to the discrete problem which enhance its stability.

A stabilized, finite element formulation for incompressible flow problems was also developed and analyzed in [10] and [11] (see also [2] and [12]). The main idea of this method consists in introducing a new unknown of the problem which is the orthogonal projection of the gradient of the discrete pressure onto the space of finite element functions. The continuity equation is then modified in a consistent way by the addition of a suitable multiple of the divergence of the difference between the pressure gradient and its projection. The method we actually employ here for the stabilization of the pressure is an anisotropic pressure-gradient-projection method, which is specially designed to be used on finite element meshes with large element aspect ratios, like those frequently employed in ocean dynamics. The anisotropically stabilized discrete problem consists in finding $\mathbf{u}_h^{n+1} = (u_h^{n+1}, v_h^{n+1}, w_h^{n+1})$, p_h^{n+1} and $\mathbf{r}_h^{n+1} = (r_1^{n+1}, r_2^{n+1}, r_3^{n+1})$ such that, for all test functions $\tilde{\mathbf{u}}_h = (\tilde{u}_h, \tilde{v}_h, \tilde{w}_h)$, q_h and $\hat{\mathbf{u}}_h = (\hat{u}_1, \hat{u}_2, \hat{u}_3)$:

$$
\begin{aligned}
\int_\Omega \frac{1}{\Delta t}(\mathbf{u}_h^{n+1} - \mathbf{u}_h^n)\,\tilde{\mathbf{u}}_h\,d\Omega \;&+\; \int_\Omega (\mathbf{u}_h^n \cdot \nabla)\mathbf{u}_h^{n+1}\,\tilde{\mathbf{u}}_h\,d\Omega \\
+\int_\Omega f(\mathbf{k}\times\mathbf{u}_h^{n+1})\tilde{\mathbf{u}}_h\,d\Omega \;&+\; \int_\Omega \nabla p_h^{n+1}\,\tilde{\mathbf{u}}_h\,d\Omega \\
+\int_\Omega (\nu_H \frac{\partial \mathbf{u}_h^{n+1}}{\partial x}\frac{\partial \tilde{\mathbf{u}}_h}{\partial x} \;&+\; \nu_H \frac{\partial \mathbf{u}_h^{n+1}}{\partial y}\frac{\partial \tilde{\mathbf{u}}_h}{\partial y} + \nu_V \frac{\partial \mathbf{u}_h^{n+1}}{\partial z}\frac{\partial \tilde{\mathbf{u}}_h}{\partial z})d\Omega \\
&=\; -\int_\Omega \frac{\rho}{\rho_0}\,\mathbf{g}\,\tilde{\mathbf{u}}_h\,d\Omega \;+\; \int_{\Gamma_s} (\tau_s^x \tilde{u}_h + \tau_s^y \tilde{v}_h)\,d\Gamma \\
&+\; \int_{\Gamma_b} (\tau_b^x(u_h^{n+1})\tilde{u}_h + \tau_b^y(v_h^{n+1})\tilde{v}_h)\,d\Gamma \\
\int_\Omega (\nabla\cdot\mathbf{u}_h^{n+1})\,\tilde{q}_h\,d\Omega \;&+\; \sum_{K\in\Omega_h}\sum_{i=1}^{3}\int_K \alpha_{K,i}\,\partial_i p_h^{n+1}\,\partial_i q_h\,d\Omega \\
-\sum_{K\in\Omega_h}\sum_{i=1}^{3}\int_K \sqrt{\alpha_{K,i}}\,r_i^{n+1}\,\partial_i q_h\,d\Omega \;&=\; 0 \\
\int_\Omega \mathbf{r}_h^{n+1}\,\hat{\mathbf{u}}_h\,d\Omega \;&-\; \sum_{K\in\Omega_h}\sum_{i=1}^{3}\int_K \sqrt{\alpha_{K,i}}\,\partial_i p_h^{n+1}\,\hat{u}_i\,d\Omega \;=\; 0
\end{aligned}
$$

Here, the stability coefficients $\alpha_{K,i}$ are computed in terms of the size of element K in the i-th direction, $h_{K,i}$, and a characteristic value of the velocity in element K in the i-th direction, $V_{K,i}$, according to the following expression, which is similar to the ones usually

employed in other stabilized formulations:

$$\alpha_{K,i} \;=\; \big(c_1\frac{\nu_i}{h_{K,i}^2} \;+\; c_2\frac{V_{K,i}}{h_{K,i}} \;+\; \frac{1}{\Delta t}\big)^{-1}, \quad \forall i=1,2,3, \quad \forall K\in\Omega_h$$

where c_1 and c_2 are given constants, $\nu_1=\nu_2=\nu_H$ and $\nu_3=\nu_V$.

4 NUMERICAL RESULTS

We present in this Section some numerical results obtained with the model just described on two test cases: the classical Ekman's spiral problem and a real-life application to the study of the flow in the vicinity of the Ebro river delta.

4.1 Ekman's flow

As a first test case, we considered the well-known problem of the flow of a viscous incompressible fluid driven by a steady wind (blowing in the direction of the y axes) and subject to the Coriolis force. For an ocean of infinite depth, an analytical solution of this problem is available, in which the flow is horizontal and varies only with depth according to:

$$u \;=\; u_0\, e^{(\pi z/D)}\cos(\frac{\pi}{4} \;+\; \frac{\pi z}{D}) \tag{17}$$

$$v \;=\; u_0\, e^{(\pi z/D)}\sin(\frac{\pi}{4} \;+\; \frac{\pi z}{D}) \tag{18}$$

In (17)-(18), $u_0=\dfrac{\mathcal{T}\,D}{\sqrt{2}\,\pi\,\nu_V}$ is the fluid velocity at the surface, $\mathcal{T}$ being the wind stress (given by (10)), and the Ekman (or friction) depth D is defined as $D=\pi\sqrt{\dfrac{2\,\nu_V}{f}}$ and is characterized by the fact that at the current at $z=-D$ has the same direction but opposite sense to that at the surface. The solution (17)-(18) exhibits some other surprising features such as a drift of 45° to the right (in the Northern hemisphere) in the current at the surface with respect to the wind direction, or the way the velocity vector turns right as depth is increased while it decreases exponentially in norm at the same time, thus forming the so called Ekman's spiral. In fact, the fluid velocity at $z=-D$ is 4.32% that at the surface.

We solved this problem on a cubic domain of side 100m, with the following values of the different constants: $\rho=1025.34\,\mathrm{kg/m^3}$, $\omega=7.292\cdot10^{-5}\,\mathrm{s^{-1}}$, $\phi=45°$ (so that $f=1.03124\cdot10^{-4}\,\mathrm{s^{-1}}$), $\nu_H=100\,\mathrm{m^2/s}$, $\nu_V=1.4\cdot10^{-2}\,\mathrm{m^2/s}$, $g=0$, $\rho_a=1.3\,\mathrm{kg/m^3}$, $C_s=1.4\cdot10^{-3}$ and $(U_{10},V_{10})=(0,10)\,\mathrm{m/s}$ (so that $\mathcal{T}=1.775\cdot10^{-4}\,\mathrm{m^2/s^2}$). The surface current is then $u_0=0.1477\,\mathrm{m/s}$ and the Ekman depth is $D=51.76\,\mathrm{m}$, so that the domain of frictional influence lies within the computational domain. In this sense, both at the lateral boundaries and at the bottom an open boundary condition was imposed.

A non-uniform mesh of hexahedral elements with $4\times4\times30$ elements was employed, which is equally spaced in the horizontal directions and refined vertically near the surface and the bottom. The steady state results obtained for the column of water at the center of the domain are shown in Figure 1, where we plot the vertical profile of the velocity in

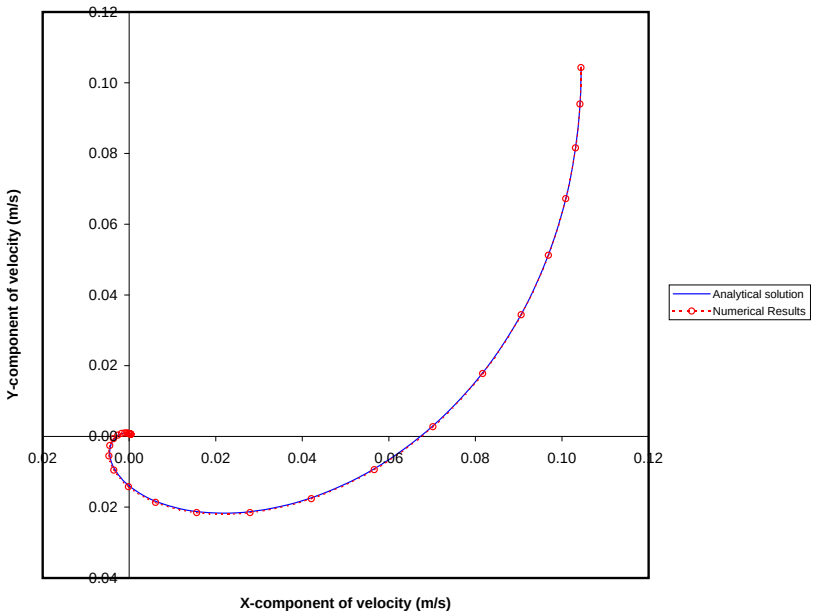

Figure 1: Vertical profile of the horizontal velocity in Ekman's flow for an ocean of infinite depth: numerical results ($\circ$) versus analytical solution (solid line).

the (u, v) plane; an exact agreement with the analytical solution (17)-(18) is observed. Figure 2 shows a perspective view of the vertical profile of the velocity vector.

When an ocean of finite depth H is considered and the solution is assumed to vanish at $z = -H$, an analytical solution also exists, but it is rather more complicated than (17)-(18). This time, the angle of veering of the velocity vector at the surface to the right of the wind direction is highly dependent on the ratio H/D. We solved this problem again but now imposing zero velocity in all directions at the bottom for three different values of the depth corresponding to $H = 100m$, $D/2$ and $D/3$, respectively. The vertical profiles of the velocity for these three cases are shown in Figure 3, where an exact agreement with the analytical solutions can again be observed.

4.2 The Ebro river delta

This application test case consists of simulating the wind driven circulation at the continental shelf around the Ebro delta. The Ebro delta is located at the transition between a (northern) narrow shelf stretch (10 km wide) and a (southern) broader shelf area (50-60 km wide). Such a topographic setting constitutes an ideal test case on complex coastlines and bathymetry for the model.

The domain considered in this study extends from Cape Salou to the Columbretas Islands off the northeastern Spanish coast and is limited by the coastline, the 600 m isobath, a northern cross-shore transect off Cape Salou and a southern cross-shore transect at the latitude of the Columbretes Islands (see Figure 4 for a satellite image of the region of interest and Figure 5 for a location map and the bathymetry of the area). The 3D unstructured computational mesh used consists of 46,963 tetrahedral elements and 12,252 nodes, whose size fits nicely to the complicated boundaries (Figure 6).

Since the focus of this numerical test is on the wind-induced circulation, the Ebro discharge was taken null, and therefore the density field plays no role and has been considered homogeneous with a value of 1025.34 kg/m^3. The wind stress forcing has been

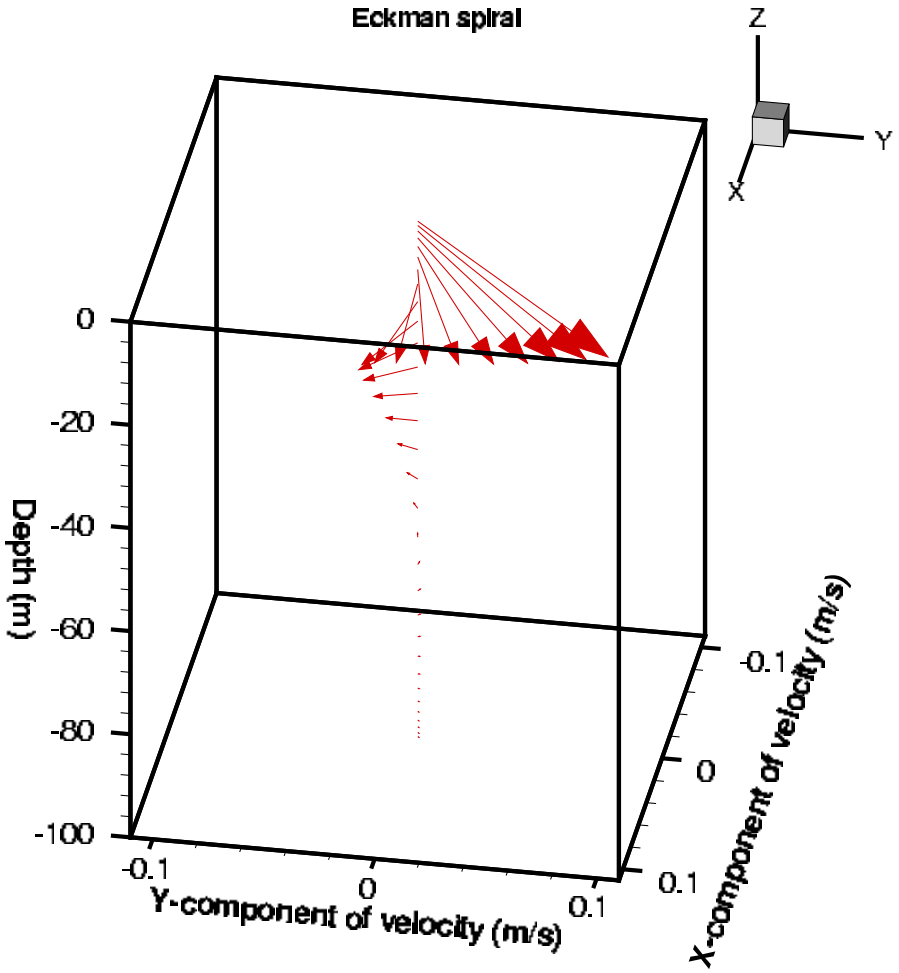

Figure 2: Perspective view of the vertical profile of the velocity vector in Ekman's flow for an ocean of infinite depth.

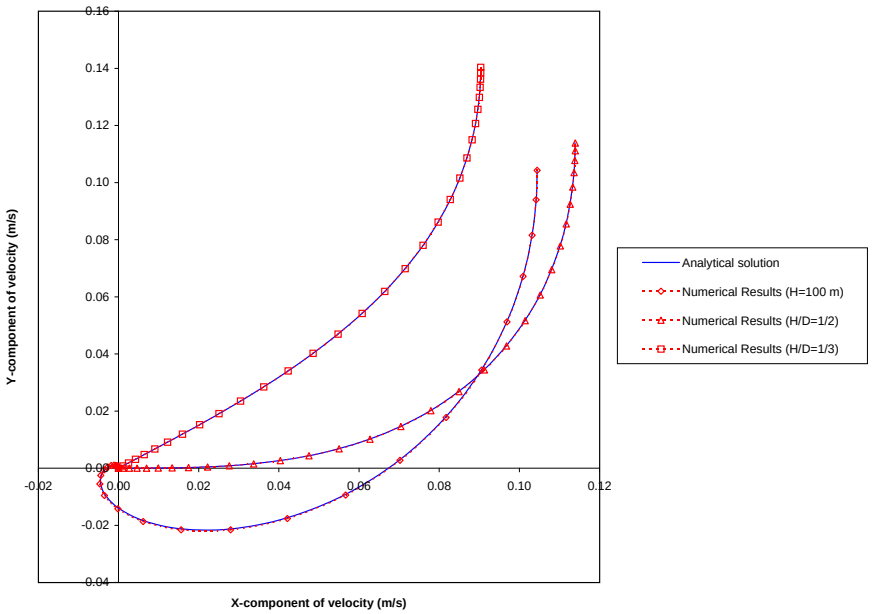

Figure 3: Vertical profile of the horizontal velocity in Ekman's flow for an ocean of finite depth H: $H = 100m$ ($\diamond$), $H = D/2$ ($\triangle$) and $H = D/3$ ($\square$) versus the analytical solution in each case (solid lines).

evaluated by using the conventional quadratic parameterization type given by (10), with an air density $\rho_0 = 1.3$ kg/m^3, a dimensionless drag coefficient $C_s = 0.0014$ and utilizing an average wind velocity vector of 10 m/s from the East.

Homogeneous Neumann conditions have been imposed for the flow on the northern and southern boundaries and a no-slip condition has been adopted for the coastal contour. The normal velocity was imposed equal to zero at the bottom and a linear relationship between the bottom stress and the near-bottom velocity has been considered to parameterize the bottom friction (equation 8), with a homogeneous bottom friction coefficient $C_b = 0.001$ kg/m^{2}s.

The horizontal and vertical eddy viscosity coefficients chosen for this case were $\nu_H = 1.0e+03$ and $\nu_V = 1.4e-01$. The following other physical constants were used: latitude 41^oN, Earth's angular velocity $7.292e-05$ s^{-1}, so that the Coriolis parameter is $f = 9.568e-05$ s^{-1}; finally, the gravity force was set equal to zero.

As a way to reproduce numerically the presence of a slope jet off the shelf edge, 1,434 time steps were performed specifying only an along-slope flow of 0.1 m/s as a boundary condition on the open sea, until a steady state was reached with a tolerance of 1.0e-05. In the first 4 steps, a direct method (LDU decomposition with skyline storage) was employed to solve the velocity-pressure matrix system, and then the next 1,430 iterations were made utilizing a fast iterative method (FGMRES with preconditioning strategy Left ILU). Finally, after adding the wind stress forcing over the free surface, 1,130 iterations were done until a new steady state was reached. In all the simulations, a time step of 10 seconds was employed and the pressure gradient matrix system was lumped to save CPU time and RAM memory.

Plotted in Figure 7 are the computed velocities at the sea surface. As can be seen, the surface marine currents are driven mainly by wind from East to West over the continental shelf, in shallow water, while along the slope the current flow follows the isobaths towards

Figure 4: The Ebro river delta: satellite image of the region of interest.

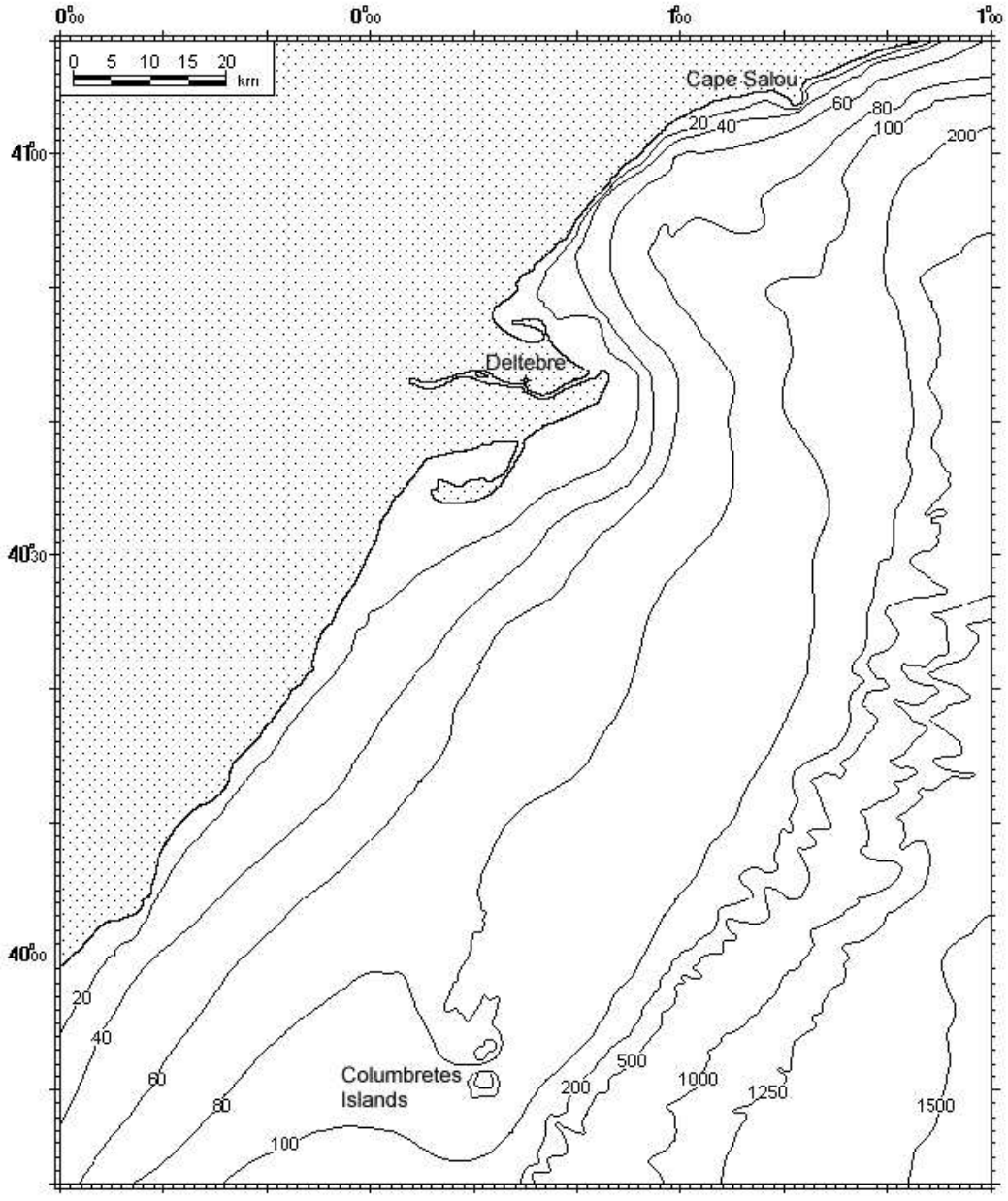

Figure 5: The Ebro river delta: location map and bathymetry.

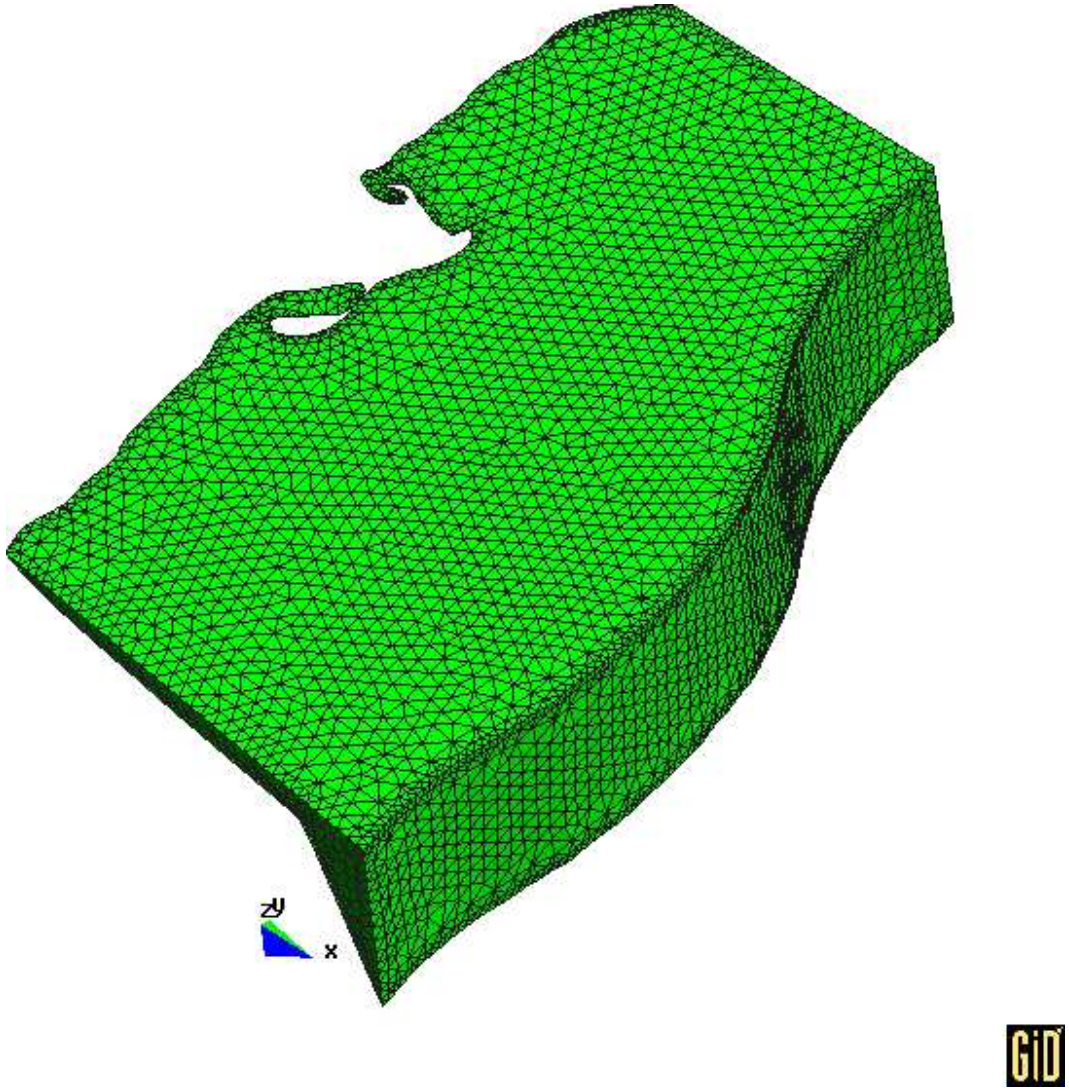

Figure 6: The Ebro river delta: 3D computational mesh of tetrahedral finite elements.

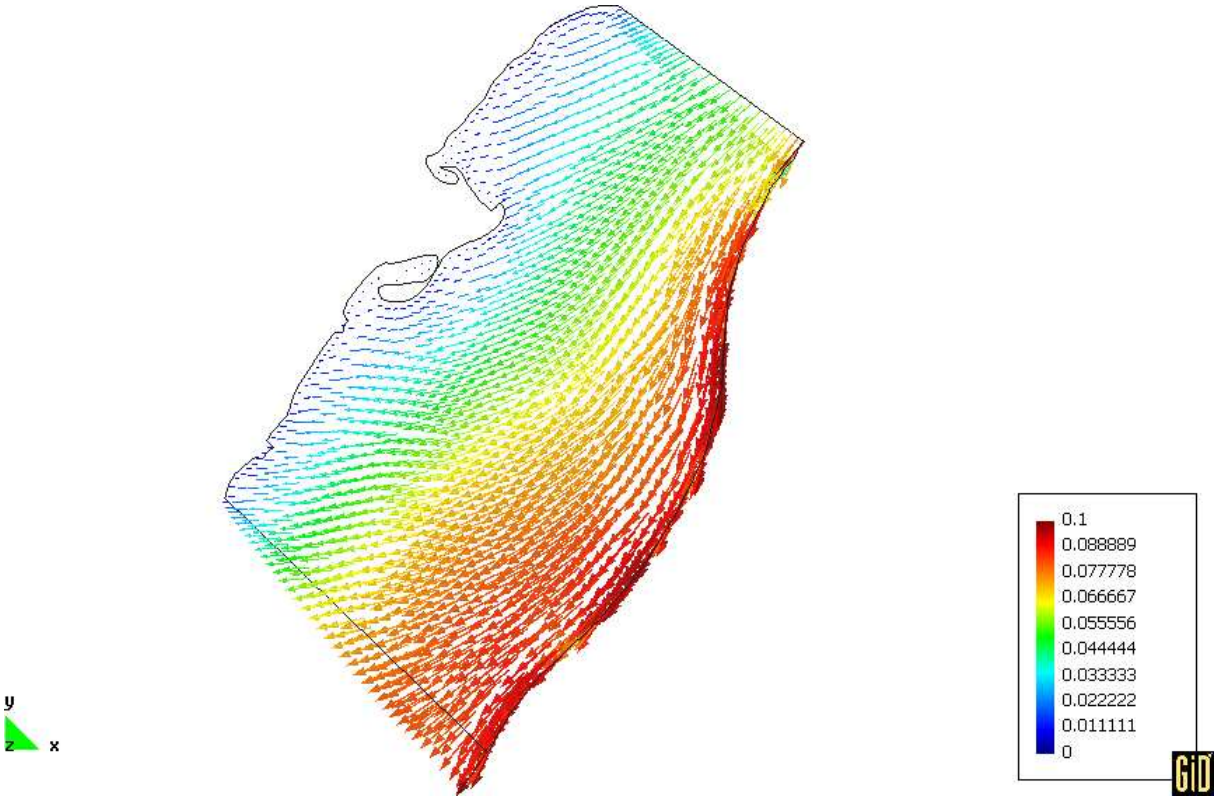

Figure 7: Velocity vectors at the sea surface.

S-SW.

Figure 8 depicts the isosurfaces of the velocity module, which attain their maximum at the open sea boundary and decrease towards the coastline. Figure 9 shows the trajectories of some selected points; as can be seen, those starting in the slope area follow closely the bathymetry, while those starting in the shelf area are more influenced by the wind drag. In Figures 6, 8 and 9, the vertical scale factor was magnified 50 times for visualization purposes.

5 CONCLUSIONS

An implicit finite element model for 3D non-hydrostatic mesoscale ocean flows has been described and applied successfully. Computationally, the conservative numerical scheme is suitable for the simulation of three-dimensional non-hydrostatic flows using fine spatial resolution and relatively large time steps. The non-hydrostatic approximation has a significant role on rapidly varying slopes and convective dominant flows. An anisotropic pressure-gradient projection method was used here to stabilize the pressure which is specially designed to be used on finite element meshes with large element aspect ratios like those frequently employed in coastal dynamics.

The combined use of finite element methods and unstructured meshes provides a great flexibility for fitting boundaries, local mesh refinements and the application of appropriate boundary condition. The numerical results obtained on the test cases presented demonstrate the robustness and accuracy of the method proposed. This model can be used efficiently for both Ocean and Coastal Engineering. It can be foreseen that finite element

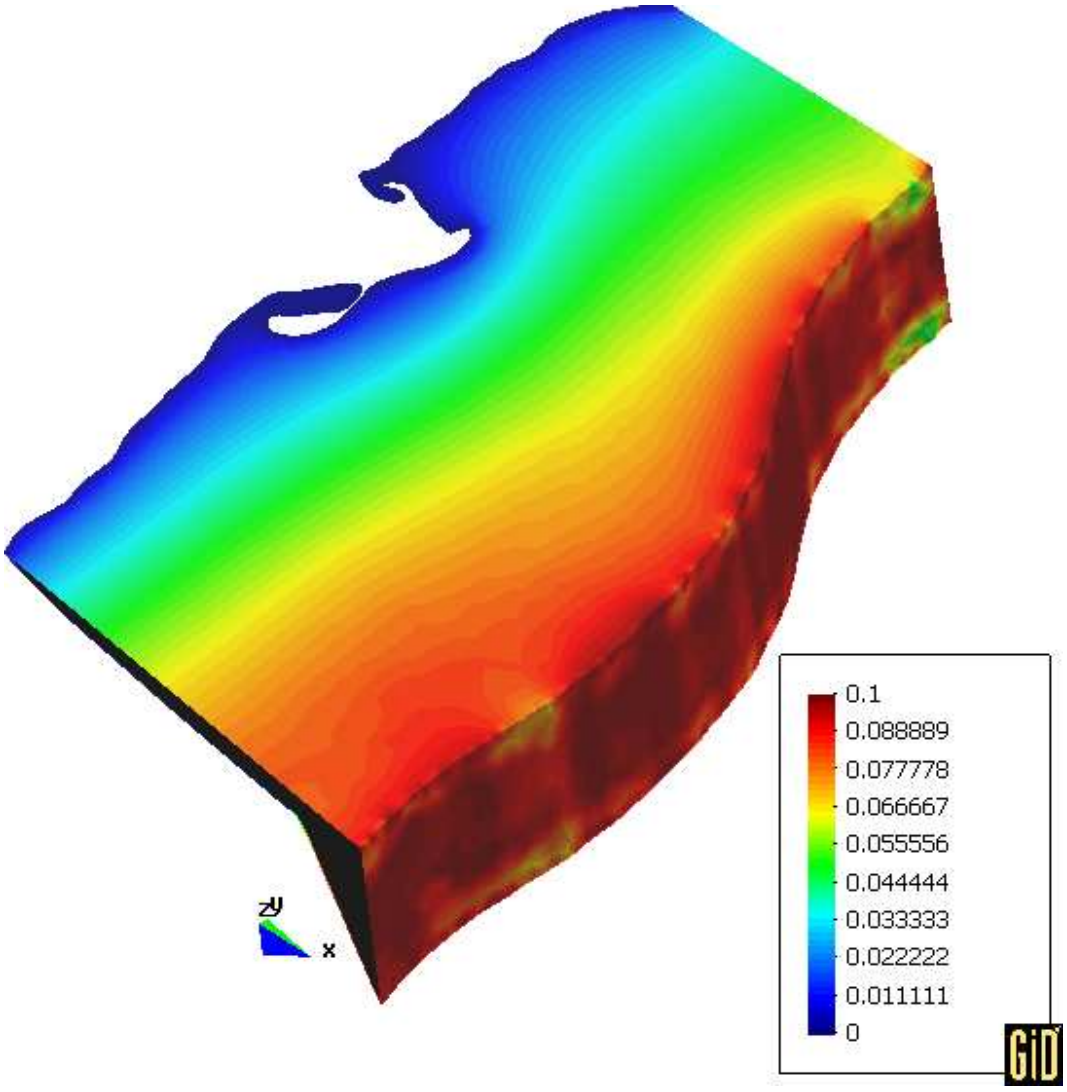

Figure 8: Isosurfaces of the velocity modulus.

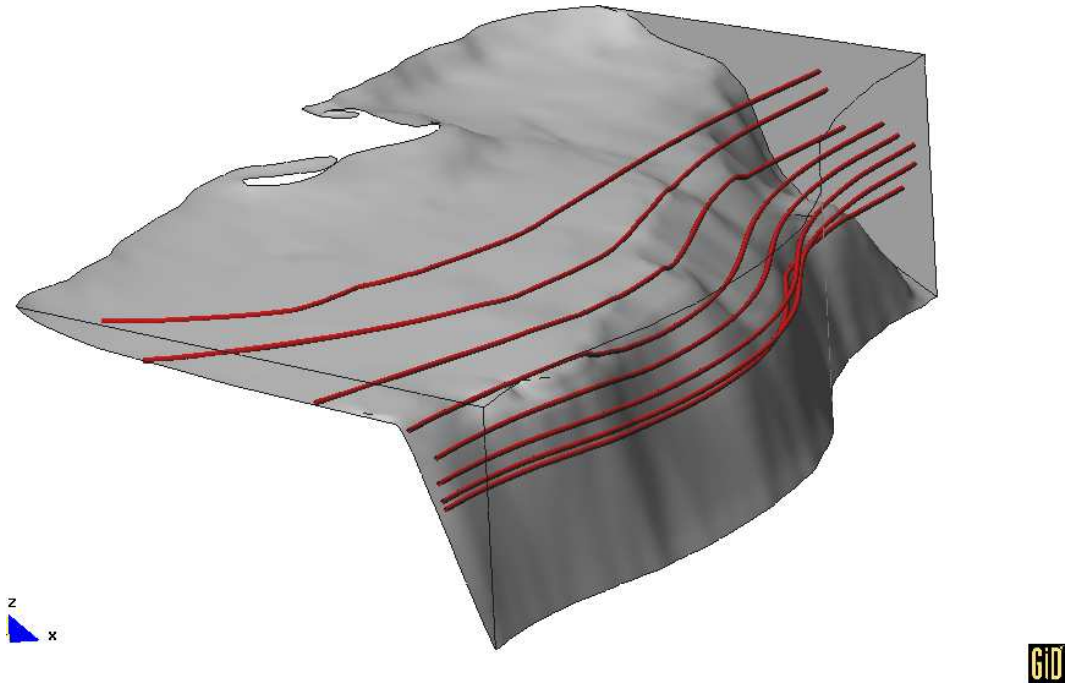

Figure 9: Some particle trajectories.

methods will supersede traditional models and will play an important role in future ocean modelling.

References

[1] G. Barrenechea and F. Valentin. An unusual stabilized finite element method for a generalized Stokes problem. *Numerische Mathematik* 2002; **92**: 635–677.

[2] J. Blasco and R. Codina. Space and time error estimates for a first order, pressure stabilized finite element method for the incompressible Navier-Stokes equations. *Applied Numerical Mathematics* 2001; **38**: 475–497.

[3] J. Blasco, R. Codina and A. Huerta. A fractional–step method for the incompressible Navier–Stokes equations related to a predictor-multicorrector algorithm. *International Journal for Numerical Methods in Fluids* 1998; **28**: 1391–1419.

[4] F. Brezzi and J. Douglas. Stabilized mixed methods for the Stokes problem. *Numerische Mathematik* 1988; **53**: 225–235.

[5] F. Brezzi and M. Fortin. *Mixed and Hybrid finite element methods*. Springer Series in Computational Mathematics, 15. Springer–Verlag, 1991.

[6] A.N. Brooks and T.J.R. Hughes. Streamline upwind/Petrov-Galerkin formulations for convection dominated flows with particular emphasis on the incompressible Navier–Stokes equations. *Computer Methods in Applied Mechanics and Engineering* 1982; **32**: 199–259.

[7] V. Casulli, P. Zanolli. Semi-implicit numerical modelling of nonhydrostatic free–surface flows for environmental problems. *Mathematical and Computer Modelling* 2002; **36**: 1131–1149.

[8] T. Chacón Rebollo. A term-by-term stabilization algorithm for the finite element solution of incompressible flow problems. *Numerische Mathematik* 1998; **79**: 283–319.

[9] T. Chacón Rebollo, D. Rodríguez Gómez. A stabilized space-time discretization for the primitive equations in oceanography. *Numerische Mathematik* 2004; **98**: 427–475.

[10] R. Codina and J. Blasco. A finite element formulation for the Stokes pro-blem allowing equal velocity-pressure interpolation. *Computer Methods in Applied Mechanics and Engineering* 1997; **143**: 373–391.

[11] R. Codina and J. Blasco. Analysis of a pressure-stabilized finite element approximation of the stationary Navier-Stokes equations. *Numerische Mathematik* 2000; **87**: 59–81.

[12] R. Codina, J. Blasco, G.C. Buscaglia and A. Huerta. Implementation of a stabilized finite element formulation for the incompressible Navier-Stokes equations based on a pressure gradient projection. *International Journal for Numerical Methods in Fluids* 2001; **37**: 419–444.

[13] R. Codina and O. Soto. Finite element solution of the Stokes problem with dominating Coriolis force. *Computer Methods in Applied Mechanics and Engineering* 1997; **142**: 215–234.

[14] S. Danilov, G. Kivman, J. Schröter. A finite–element ocean model: principles and evaluation. *Ocean Modelling* 2004; **6**: 125–150.

[15] C. Dawson, J. Proft. Coupled discontinuous and continuous Galerkin finite element methods for the depth-integrated shallow water equations. *Computer Methods in Applied Mechanics and Engineering* 2004; **193**: 289–318.

[16] M. Espino, M.A. Maidana, A. Sánchez-Arcilla, A. German. Hydrodynamics in the Huelva estuary. Tidal model calibration using field data. *Journal of Waterway, Port, Coastal and Ocean Engineering*. 2004, submitted.

[17] M. Espino, A. Sánchez-Arcilla, M.A. García. Wind-induced mesoscale circulation off the Ebro delta, NW Mediterranean: a numerical study. *Jour. of Marine Systems* 1998; **16**: 235–251.

[18] G.J. Fix. Finite element model for ocean circulation problems. *SIAM Journal on Applied Mathematics* 1975; **29**: 371–387.

[19] L.P. Franca and S.L. Frey. Stabilized finite element methods: II. The incompressible Navier-Stokes equations. *Computer Methods in Applied Mechanics and Engineering* 1992; **99**: 209–233.

[20] L.P. Franca and T.J.R. Hughes. Convergence analyses of Galerkin least-squares methods for symmetric advective-diffusive forms of the Stokes and incompressible Navier-Stokes equations. *Computer Methods in Applied Mechanics and Engineering* 1993; **105**: 285–298.

[21] P.M. Gresho. On the theory of semi-implicit projection methods for viscous incompressible flow and its implementation via a finite element method that also introduces a nearly consistent mass matrix. *International Journal for Numerical Methods in Fluids* 1990; **11**: 587–620.

[22] J.L. Guermond and L. Quartapelle. On stability and convergence of projection methods based on pressure Poisson equation. *International Journal for Numerical Methods in Fluids* 1998; **26**: 1039–1053.

[23] F. Guillén-González, D. Rodríguez-Gómez. *Bubble finite elements for the primitive equations of the ocean*. Numerische Mathematik, 2005, to appear..

[24] M.B. Koçyigit, R. A. Falconer, B. Lin. Three-dimensional numerical modelling of free surface flows with non-hydrostatic pressure. *International Journal for Numerical Methods in Fluids* 2002; **40**: 1145–1162.

[25] C. Le Provost. *On the use of finite element methods for ocean modelling*. In: J.J. O'Brien (Ed.), Advanced Physical Oceanographic Numerical Modelling, D. Reidel Publishing, 1986, p. 557–580..

[26] D.Y. Le Roux, G.F. Carey. Dispersion analysis of the least-squares finite-element shallow-water system. *International Journal for Numerical Methods in Fluids* 2003; **42**: 607–622.

[27] P. Lin, C.W. Li. A σ-coordinate three-dimensional numerical model for surface wave propagation. *International Journal for Numerical Methods in Fluids* 2002; **38**: 1045–1068.

[28] J. Macías, C. Parés, M.J. Castro. Improvement and generalization of a finite element shallow-water solver to multi-layer systems. *International Journal for Numerical Methods in Fluids* 1999; **31**: 1037–1059.

[29] M.A. Maidana, J.J. Naudin, M. Espino, M.A. García, A. Sánchez-Arcilla. Feasibility and usefulness of diagnostic calculations of the mean circulation in the vicinity of the Ebro mouth. Model tests against field data. *Continental Shelf Research* 2002; **22**: 229–245.

[30] C.Y. Shen, T.E. Evans. A free-surface hydrodynamic model for density-stratified flow in the weakly to strongly non-hydrostatic regime. *Journal of Computational Physics* 2004; **200**: 695–717.

[31] G. Stelling, M. Zijlema. An accurate and efficient finite-difference algorithm for non-hydrostatic free-surface flow with application to wave propagation. *International Journal for Numerical Methods in Fluids* 2003; **43**: 1–23.

[32] H. Yuan, C.H. Wu. A two-dimensional vertical non-hydrostatic σ model with an implicit method for free-surface flows. *International Journal for Numerical Methods in Fluids* 2004; **44**: 811–835.

[33] O.C. Zienkiewicz, P. Ortíz. A split-characteristic based finite element model for the shallow water equations. *International Journal for Numerical Methods in Fluids* 1995; **20**: 1061–1080.